Supercontinuum generation in the vacuum ultraviolet through dispersive-wave and soliton-plasma interaction in a noble-gas-filled hollow-core photonic crystal fiber

A. Ermolov,* K. F. Mak, M. H. Frosz, J. C. Travers, and P. St. J. Russell
Max Planck Institute for the Science of Light, Günther-Scharowsky-Strasse 1, 91058 Erlangen, Germany
(Received 13 March 2015; published 14 September 2015)

We report on the generation of a three-octave-wide supercontinuum extending from the vacuum ultraviolet (VUV) to the near infrared, spanning at least 113–1000 nm (i.e., 11−1.2eV), in He-filled hollow-core kagome-style photonic crystal fiber. Numerical simulations confirm that the main mechanism is an interaction between dispersive-wave emission and plasma-induced blue-shifted soliton recompression around the fiber zero dispersion frequency. The VUV part of the supercontinuum, the modeling of which proves to be coherent and possesses a simple phase structure, has sufficient bandwidth to support single-cycle pulses of 500 asec duration. We also demonstrate, in the same system, the generation of narrower-band VUV pulses through dispersive-wave emission, tunable from 120 to 200 nm with efficiencies exceeding 1% and VUV pulse energies in excess of 50 nJ.

DOI: 10.1103/PhysRevA.92.033821 PACS number(s): 42.65.Ky, 32.80.Fb, 42.65.Re, 42.81.Dp

I. INTRODUCTION

Vacuum-ultraviolet (VUV) light (100–200 nm) has a wide range of applications. Broadband coherent VUV sources could be used to produce subfemtosecond pulses for precise—temporal, spectral, and spatial—excitation of the electronic resonances of many atoms, molecules, and solids, and form the basis for advanced time-resolved pump-probe spectroscopy [1–3] or the control of individual electronic wave packets [4,5]. Techniques such as attosecond transient absorption spectroscopy [6], photoemission spectroscopy [7], and photoionization mass spectroscopy [8] would directly benefit. Other applications include seeding free-electron lasers [9,10] and control of chemical reactions [11].

Existing spatially coherent sources in the VUV region include large-scale synchrotrons and free-electron lasers, or inefficient, and often elaborate, discrete frequency-conversion systems. Examples include second harmonic generation in exotic crystals, such as SrB_4O_7 [12], third harmonic generation [13], and four-wave mixing [8,14] in gases. These techniques usually produce VUV radiation with a narrow relative frequency bandwidth and cannot be used to generate coherent subfemtosecond pulses for the applications described above.

Here we make use of soliton dynamics in gas-filled kagome-style photonic crystal fibers (kagome-PCFs) [15–17] to efficiently generate tunable, coherent, ultrafast pulses from 120 nm to beyond 180 nm (11−7eV). In addition, we show that in He-filled kagome-PCF, this emission can evolve into a flat supercontinuum (SC) spanning from at least 113 to 1000 nm (11−1.2eV)—over three octaves. This is the shortest wavelength VUV SC generated in any system. Although soliton dynamics in kagome-PCF have been widely explored [16,17], showing, among many effects, a straightforward route to the generation of tunable deep-UV light [18,19], the mechanism demonstrated in this paper, based on a combination of resonant dispersive-wave emission and soliton-plasma interactions, is different.

II. BACKGROUND

SC generation has been studied in glasses [20], gases [21], and liquids [22]. It is well established that in bulk materials the high-frequency SC edge scales with the frequencies of the ultraviolet electronic resonances of the medium, which are directly related to the ionization potential (I_p) [23]. This is primarily due to strong material dispersion [24]. Materials with the highest I_p, however, also have the lowest values of nonlinearity [25]; thus in free space VUV SC generation requires very intense laser systems and filamentation, limiting the repetition rate and degrading the spatial coherence. With 33-GW few-cycle pump pulses in argon, the SC edge has reached ∼210 nm at the 30-dB level [26]. Alternatively, the use of plasma defocusing of single-cycle pulses in Ne yielded a UV SC extending from 150 to 300 nm [27]. Truly continuous extensions into the VUV have required terawatt pulses and spatially incoherent multifilamentation; the shortest wavelength achieved in that regime is ∼150 nm at the 40-dB level in Ar [28].

Solid-core PCFs [29] enhance the generation of broad and flat SCs [30,31] by providing extended light-matter interaction lengths and anomalous (i.e., negative) group velocity dispersion (GVD) at common near-infrared pump wavelengths. Thus effects such as soliton-effect self-compression to few-cycle or even subcycle pulses [16,32,33], soliton fission [34–36], and resonant dispersive-wave emission at higher frequencies [18,19,36–38] come into play. These processes have been harnessed to extend the SC pumped by near-infrared laser pulses into the deep UV. Glass-core optical fibers cannot, however, transmit in the VUV, the shortest wavelength SC edge achieved in solid-core PCF being 280 nm in silica-based fibers [39] and 200 nm in PCFs made from ZBLAN glass [40].

Gas-filled kagome-PCF [15–17] [see scanning electron micrograph (SEM) in Fig. 1(a)] permits broadband low-loss transmission at core diameters of a few tens of micrometers. In such small cores the anomalous waveguide dispersion is large enough to balance the normal dispersion of the filling gas at pressures of a few bar. This makes it possible to operate with anomalous dispersion at pump wavelengths in the near infrared (NIR) while benefiting from VUV transmission [41] and very high damage thresholds. Figure 1(a) shows the transmission loss of a 28-μm kagome-PCF from 600 to 1000 nm, and the inset of Fig. 1(c) shows the dispersion from the VUV to near IR when it is filled with 28 bar of He. The zero dispersion wavelength (ZDW) is at 370 nm and the dispersion at 800 nm is $-0.65\ \mathrm{fs}^2/\mathrm{mm}$.

*alexey.ermolov@mpl.mpg.de

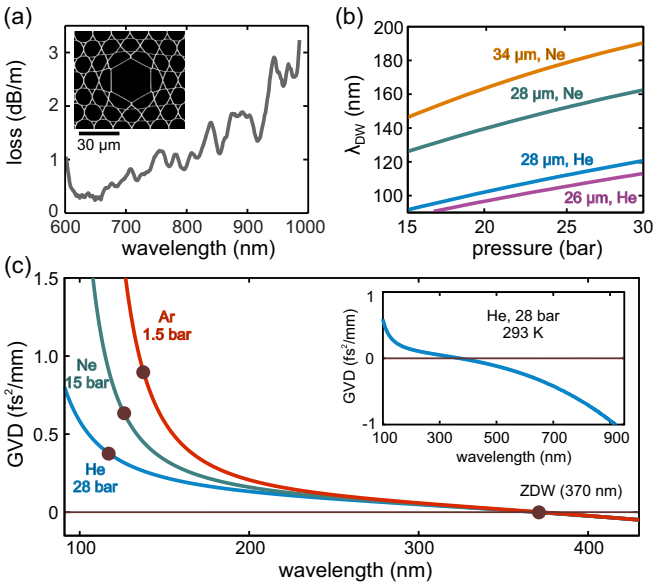

FIG. 1. (Color online) (a) Measured loss of kagome-PCF with a core diameter of 28 μm. The inset shows an SEM of a typical kagome-PCF. (b) Dependence of DW wavelength on pressure for various gases and fiber core diameters (calculated according to pulse duration 35 fs, pulse energy 4 μJ, 3.5μJ, 5μJ, and 5 μJ for orange, green, blue, and purple curves, respectively). (c) Dispersion characteristics of the kagome-PCF in (a), obtained for three different gases; the pressures were chosen to yield the same ZDW in each case. The brown dots in the vicinity of 150 nm denote the DW wavelength for each case. The inset shows the calculated dispersion characteristics from the VUV to the NIR when the 28-μm fiber is filled with 28 bar of He.

Three mechanisms for up-shifting the frequency of pump pulses at 800 nm in gas-filled kagome-PCF have been previously reported: (i) efficient, coherent, and tunable dispersive-wave (DW) emission (also known as resonant or Cherenkov radiation in earlier publications) to the deep-UV and visible regions (180–550 nm) [18,19]; (b) the soliton self-frequency blueshift, driven by photoionization [42–45]; and (c) impulsive Raman scattering [41]. The last of these made use of a hydrogen-filled kagome-PCF, where impulsively excited Raman coherence resulted in strong spectral broadening into the VUV (124 nm at the 40-dB level) of DWs initially generated at ∼180 nm. However, hydrogen has an I_p similar to argon, so direct generation of light at wavelengths below 120 nm is unlikely, and additionally, the VUV SC is not especially flat.

Here we report a technique for generating a bright, flat VUV SC extending to below 113 nm, as well as extending high-energy wavelength-tunable VUV dispersive-wave emission down to 120 nm.

The transfer of radiation, from a self-compressed soliton pump pulse to a DW at a certain up-shifted frequency, is phase matched by higher-order dispersion [46–48]. The process can be understood as cascaded four-wave mixing [49]. Neglecting the nonlinear phase shift and dispersion terms higher than third order, the DW frequency ω_{dw} is given by

$$\omega_{dw} = \omega_{sol} + 3|\beta_2|/\beta_3 = 3\omega_{zd} - 2\omega_{sol}, \qquad (1)$$

where ω_{zd} is the frequency of the ZDW and ω_{sol} is the central frequency of the pump soliton; β_2 is the GVD, and β_3 is the third-order dispersion, both at the pump frequency. This indicates that VUV light (<200 nm) can be generated from a NIR pump pulse at 800 nm if the ZDW is in the UV region (<400 nm). According to Eq. (1), kagome-PCFs filled with different gases will emit DWs at the same UV frequency ω_{dw} if the pressure is adjusted so that they share the same ZDW (or equivalently, the same value of $|\beta_2|/\beta_3$). In practice this is not precisely true: at frequencies close to the electronic transitions, the group velocity dispersion varies rapidly [Fig. 1(c)], so that higher-order dispersion (i.e., β_4 and higher) alters the phase-matching condition in Eq. (1). The predicted wavelengths of the DWs, taking account of higher-order dispersion, are plotted as a function of pressure in Fig. 1(b) for two different gases and three different core diameters. In keeping with the general trend in SC generation [23], the shortest VUV wavelengths can be reached only with the lightest (i.e., with the highest I_p) gases (Ne and He), resulting in tunability from 100 to 200 nm.

III. EXPERIMENT

The experimental setup is shown in Fig. 2. Linearly polarized, 35-fs pump pulses at 800 nm and 1-kHz repetition rate, generated by a Ti:sapphire amplifier (Coherent, Legend Elite), were reflected by two pairs of chirped mirrors to compensate for the GVD induced by the subsequent spatial filter, achromatic focusing lens, and input window. (The second pair was placed right before the gas cell.) A combination of thin-film polarizer (TFP) and half-wave plate ($\lambda/2$) allowed the input energy to be controlled from 100's of nanojoules to 10's of microjoules. The spatial filter consisted of focusing (L1) and collimating (L2) lenses and a 100-μm aperture (A) between them. We mounted several kagome-PCFs (F) with different core sizes between two gas cells [16,17] and filled them with He and Ne gas at pressures of up to 30 bar. The gas cells were connected by plastic tubing, with the kagome-PCF running through it. To deliver light in and out of the gas cells, fused silica (FS) and MgF_2 (MgF) windows, respectively, were sealed into the cell faces. The beam was focused onto the fiber tip by an achromatic lens (L3). The gas cells were evacuated and purged several times before being filled with

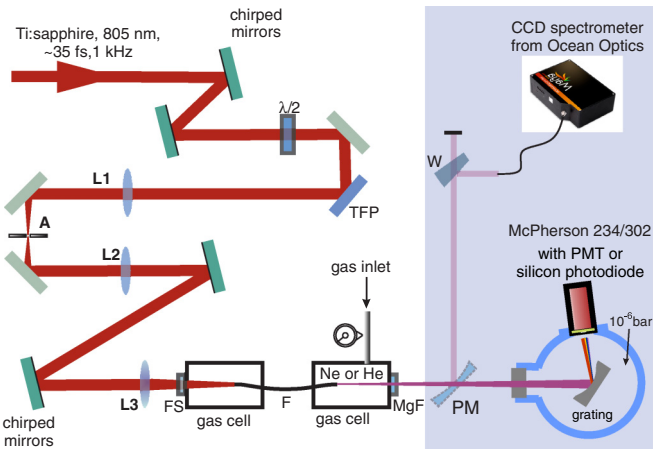

FIG. 2. (Color online) Schematic of experimental setup. The elements are described in the main text.

the chosen gas at constant pressure. For VUV diagnostics the gas cell was connected to a McPherson vacuum spectrometer (234/302) via a bellows. The spectrometer was evacuated by a turbomolecular vacuum pump down to microbar pressure. The VUV detectors used were either a sodium salicylate scintillator and photomultiplier tube (McPherson) or a silicon photodiode (Opto Diode Corporation), which had been absolutely calibrated between 90 and 220 nm using a synchrotron light source. To measure the entire spectrum including visible and near-IR parts, the McPherson spectrometer was replaced by a parabolic mirror (PM) and fused silica wedge (W) to collimate and attenuate the beam coming out of the fiber and steer it to an Ocean Optics MayaPro CCD spectrometer. The measured spectrum was corrected for the spectrometer response and wavelength-dependent diffraction from the output of the fiber.

The VUV spectra for Ne pressures of 26 and 21 bar are shown in Fig. 3(a)(i,ii), where a 34-μm-diameter kagome-PCF was used with 4-μJ pump energy. The results show that the DW frequency can be shifted into the VUV purely by pressure tuning (tuning out to 550 nm using Ne and heavier gases has been previously demonstrated [20]). Furthermore, additional DWs at even shorter wavelength are also emitted into higher-order modes [50], as seen, for example, in the red curve [marked – (i) in Fig. 3(a)], where the peak at 154 nm corresponds to a DW emitted into the HE_{12} mode [confirmed by numerical modeling – black curve – (iv)]. Reducing the core size to 28 μm and increasing the pressure to 21 bar shifts the ZDW further into the VUV, resulting in DW emission at 145 nm [Fig. 3(a)(iii)]. We have performed the measurements of energy contained in these peaks. To do this the PMT of the McPherson spectrometer was replaced by a silicon photodiode from Opto Diode Corporation (Fig. 2). The input slit of the McPherson spectrometer was removed to allow the entire beam to enter (effectively utilizing the output of the fiber as the input slit) and the output slit was set up to have 1-nm resolution (verified using a mercury lamp). We corrected the measured spectrum using the known photodiode responsivity, grating efficiency, and MgF_2 window transmission. To eliminate the effect of scattered light in the monochromator chamber, the measurements were repeated with exactly the same parameters for each spectrum, but with the chamber flushed with air to absorb the VUV or with a variety of glass and crystal filters. This signal was then subtracted from the original to avoid overestimation of the VUV power. The measured energy varied from 5 to 50 nJ in a range 110–200 nm, depending on the fiber diameter, length, and phase-matching conditions defined by pump energy, gas species, and pressure. It corresponds to a conversion efficiency to the VUV of ∼1%, significantly higher than obtained using the other approaches discussed in the Introduction.

Switching to 28.2 bar He in the kagome-PCF with core diameter 28 μm and pumping with 5-μJ energy, the DW peak can be shifted to 135 nm [Fig. 3(b)(i)]. Using an even smaller core diameter (26μm) with 28 bar He, the DW could be tuned down to 120 nm [Fig. 3(b)(ii)] for 3.5-μJ pump energy.

These He spectra are not discrete DW peaks but in fact broad supercontinua extending from below 113 nm to beyond the range of the VUV spectrometer. Note that the spectra in Fig. 3(b) are displayed on a linear scale; the inset shows them

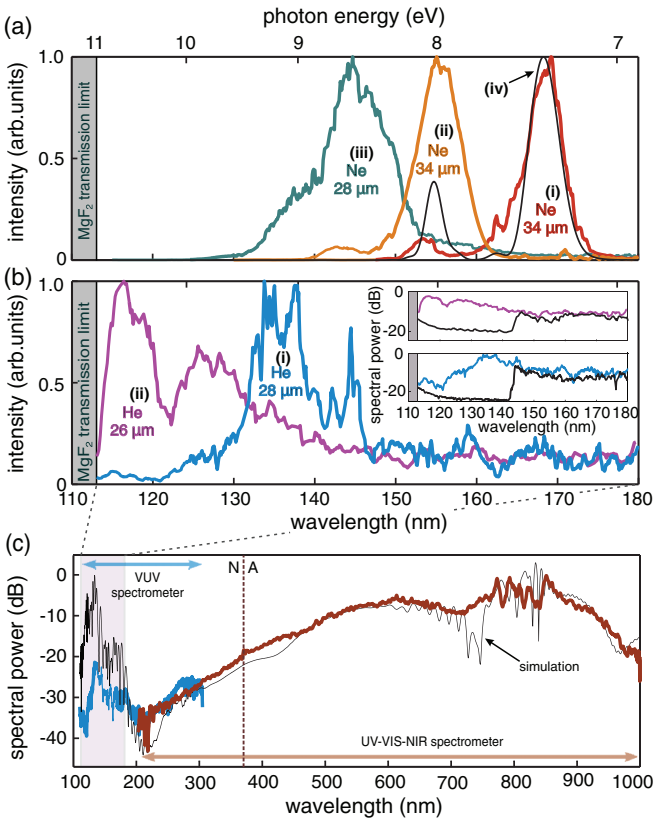

FIG. 3. (Color online) (a) Experimental spectra of coherent ultrashort pulses generated by DW emission in Ne-filled kagome-PCF for parameters given in the text (each curve is individually normalized). The red and orange curves were taken at different gas pressures, all other parameters being fixed. The numerical simulation [solid black line marked (iv)] reproduces the experimental red curve and shows a small peak at 154 nm corresponding to DW emission into the HE_{12} mode. (b) The VUV SC in He (linear scale) for core diameters of (i) 28 μm and (ii) 26 μm; (inset) the same data on a logarithmic scale, including the spectra recorded through a sapphire filter (black lines). (c) The full SC corresponding to (b)(i). The blue curve was measured using the VUV spectrometer and the brown curve using the UV-NIR spectrometer. The solid black line is the simulated spectrum. The dashed vertical line marks the ZDW (N = normal, A = anomalous GVD).

on a logarithmic scale, emphasizing the extreme (<10 dB) flatness of these supercontinua across the VUV. The 113-nm short-wavelength cutoff is caused by the absorption edge of the MgF_2 window; the spectra probably extend to even shorter wavelengths. The measurement was repeated with a sapphire window placed in front of the spectrometer input slit, cutting the signal below 145 nm and confirming that it was real and not due to stray light [solid black lines in Fig. 3(b), inset]. For the remainder of this article we consider the parameters of Fig. 3(b)(i). The full extent of the SC, which extends into the infrared, is plotted in Fig. 3(c), showing that it is continuous from 113 nm to beyond 1000 nm with 35-dB flatness—a spectral range exceeding three octaves. This is the shortest wavelength edge of any continuously extending supercontinuum reported to date.

TABLE I. Coefficients of Eq. (3) for helium at 1 bar and 273 K.

$B_1 = 2.16463 \times 10^{-5}$	$C_1 = -6.8077 \times 10^{-4}$
$B_2 = 2.10561 \times 10^{-7}$	$C_2 = 5.13251 \times 10^{-3}$
$B_3 = 4.75093 \times 10^{-5}$	$C_3 = 3.18621 \times 10^{-3}$

IV. THEORY AND DISCUSSION

To understand the nonlinear dynamics, we numerically simulated the propagation of the pulse using a multimode, carrier-resolved, unidirectional propagation equation described in detail in [50]. We included the Kerr effect, self-focusing, ionization, and plasma effects.

The nonlinear refractive index data was taken from [51], and the full modal dispersion were calculated using the Marcatili model for capillaries [52], which has previously been shown to be valid in the near-IR to deep-UV range [16]:

$$n_{nm}(\omega) = \sqrt{n_0^2(\omega) - \frac{u_{nm}^2}{k^2 a^2}}, \tag{2}$$

where n_0 is the refractive index of the gas, $u_{\rm nm}$ is the nth root of the $(m-1)$th order Bessel function of the first kind, $k = \omega c$, and a is the core radius (defined as the flat-to-flat distance for the hexagonal structure of the kagome-PCF core). For the refractive index of neon, we used the Sellmeier equation given in Ref. [53]. To describe the propagation of light at very high frequencies in helium, we developed a modified Sellmeier equation from published refractive index data down to 90 nm [54]:

$$n_0^2(\lambda) - 1 = \rho \sum_{i=1}^{3} \frac{B_i \lambda^2}{\lambda^2 - C_i}, \tag{3}$$

where ρ is the gas density relative to 1 bar at 273 K, λ is the wavelength in micrometers, and the values of B_i and C_i are given in Table I.

For the photoionization rate we used the PPT (Perelomov-Popov-Terent'ev) model [55], modified with the Ammosov-Delone-Krainov (ADK) coefficients [56]. Our model for plasma polarization closely follows that reported in [57].

The initial conditions for the numerical simulations were obtained from frequency-resolved optical gating (FROG) traces of the pump laser pulses. The simulations show excellent agreement with experiment. Two examples are provided by the full black curves in Figs. 3(a) and 3(c), demonstrating agreement both for discrete DW peaks using Ne [Fig. 3(a)] and for the full VUV-NIR SC [Fig. 3(c)]. In the second case, the discrepancies in the VUV—which we note are only in terms of spectral power and not spectral features—are most likely caused by fiber loss acquired during propagation subsequent to the VUV generation point, which is unknown in this spectral region.

Figure 4 shows the results of detailed numerical simulations for 28.2 bar He in a 28-μm-diameter kagome-PCF pumped with 5 μJ [the case in Figs. 3(b)(i) and 3(c)]. Over the first 12.5 cm of propagation, the pump pulse, corresponding to soliton order $N = 4.5$, undergoes self-compression [58]. In the spectral domain this initially results in approximately symmetric broadening due to self-phase modulation [marked (i) on

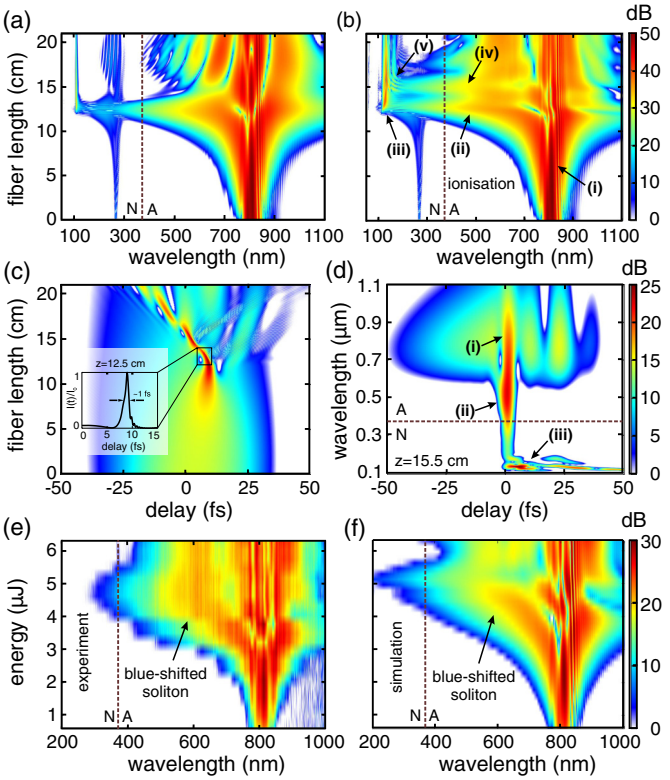

FIG. 4. (Color online) (a) Simulated spectral evolution for parameters given in the text, without ionization. (b) Same as (a) but with ionization. (c) Temporal evolution corresponding to (b); the inset shows the pulse profile at the point of maximum compression. (d) The spectrogram of the simulations in (b,c) at 15.5 cm. (e) Experimental and (f) numerical spectral evolution as a function of pump energy at the 16-cm point. The dashed lines in (a,b,d,e,f) mark the ZDW (N = normal, A = anomalous GVD).

Fig. 4(b)] that is continuously phase compensated by anomalous dispersion. The resulting temporal self-compression is clearly evident in Fig. 4(c), showing that the initial 35-fs pump pulse is compressed to a subcycle duration of less than 1 fs. This extreme compression is aided by self-steepening, leading to an optical shock [59]. The resulting blue-enhanced spectrum seeds the high-frequency DW emission, significantly increasing the conversion efficiency [18,60]. This is especially important for the frequency up-conversion into the VUV. While we do not directly measure the extremely short self-compressed pulse duration, we can confidently infer that it is produced within the fiber because it is essential for VUV DW generation and is also supported by rigorous numerical modeling.

To emit a DW in the far-VUV (~120 nm), the core size and pressure were reduced so that the ZDW shifted to shorter wavelength. This causes the perturbation due to higher-order dispersion ($\beta_3/|\beta_2|$) at the pump wavelength (800 nm) to weaken. As a result, soliton-effect compression is less disturbed and shorter self-compressed pulse durations can be reached. Reducing the pressure also diminishes the nonlinearity so that more energy is required for pulse self-compression. For both of these reasons the self-compressed peak intensity increases such that it can be sufficient to partially ionize the gas [42,44]. In kagome-PCF, due to the anomalous

dispersion, this leads to a soliton self-frequency blueshift [43–45] by over several hundred nanometers. This mechanism is crucial for enhancing the VUV emission. Figure 4(b) shows the characteristic spectral signature of a blue-shifted soliton [marked (ii)], and the spectrogram in Fig. 4(d) confirms this [Fig. 4(d) – marked (ii)]. This leads to a much stronger VUV signal [marked (iii) in Figs. 4(b) and 4(d)] compared to the case when ionization is switched off [compare Fig. 4(a) to Fig. 4(b)], because the pump soliton has a stronger overlap with the DW frequency [61]. The emission is also at a longer wavelength (130 nm as opposed to 115 nm), in agreement with Eq. (1), because the pump soliton has shifted to a higher frequency.

Figures 4(e) and 4(f) show the experimentally measured and numerically simulated evolution of the blue-shifting solitons with increasing pulse energy (1-6 μJ) for the parameters in Figs. 3(b)(i) and 3(c). Experiment and simulation agree very well, the blue-shifting soliton extending down to 400 nm, where the shift is cancelled due to its encountering the ZDW. This cancellation, analogous to the cancellation of the Raman soliton self-frequency shift at long wavelengths in solid-core fibers [62], is caused by the emission of DWs in the normal dispersion region at higher frequencies. As the DW is emitted, the soliton recoils due to energy conservation—the recoil can be described as the Stokes side of a cascaded four-wave mixing process [49]. From Fig. 4(b) we see that the soliton can subsequently reshape, blueshift again [Fig. 4(b)(iv)], and emit further DWs [Fig. 4(b)(v)]. This is confirmed by further detailed analysis of the spectrograms. In this way the soliton "bounces" several times off the zero dispersion point, each time emitting a DW in the vacuum ultraviolet. The effect of multiple DW emission is to significantly broaden the emitted spectral width. Since the role of plasma increases when phase matching moves to shorter-wavelength DWs, the broadening effect of the bouncing solitons explains the clear trend observable in Figs. 3(a) and 3(b) of increasing DW bandwidth as the DW peak is emitted at shorter wavelengths [Figs. 3(a) and 3(b)].

In the extreme case, the strong interaction between plasma-induced, blue-shifted soliton recompression and "bouncing" off the ZDW and the emission of multiple DWs in the fundamental mode, in addition to emission into a few higher-order modes [50], is a mechanism capable of forming a continuous SC extending from below 113 nm to beyond 1000 nm, as shown in the experimental results of Fig. 3(c). Note also that Figs. 3 and 4 represent the numerical data on a wavelength scale, for consistency with experimental measurements; however, the same propagation plot as in Fig. 4(b) is shown in Fig. 5(b), but on a frequency scale which illuminates the VUV supercontinuum much more clearly.

Note that the SC emission remains temporally and spatially coherent and is predominantly in the fundamental mode. Although the first few HE_{1n} modes also play a role, their spatial variation is weak and the spectrum is almost perfectly spatially homogeneous. A series of numerical simulations with different quantum and laser noise seeds, following [63], can be used to estimate the complex degree of first-order coherence, which can be simplified to

$$|g^{(1)}_{pq}(\omega)| = \left| \frac{\langle E^*_p(\omega) E_q(\omega) \rangle}{\langle |E_p(\omega)|^2 \rangle} \right|, \quad (4)$$

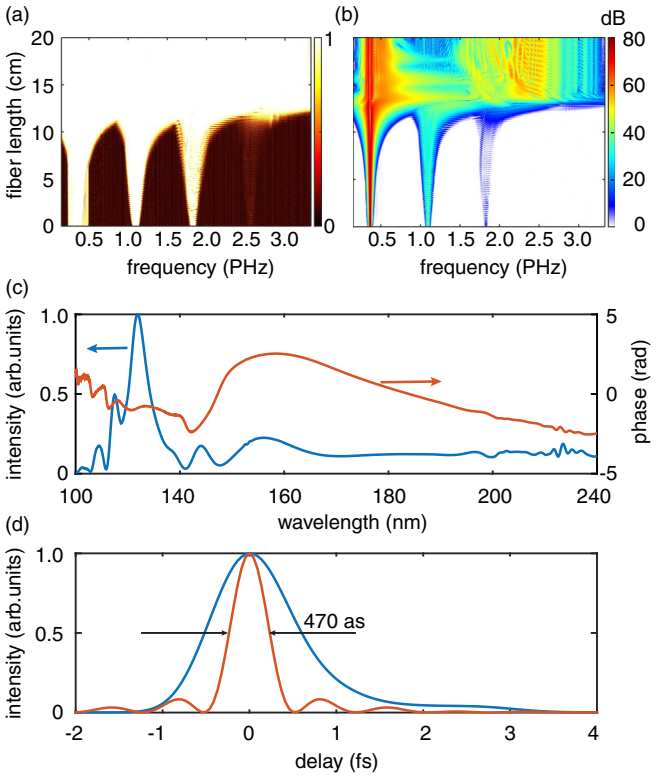

FIG. 5. (Color online) (a), (b) Simulated complex degree of first-order coherence and corresponding spectral propagation plot. The parameters are the same as in Fig. 3(b)(i) and Fig. 4(b), but the evolution is represented on a frequency scale. (c) The spectral intensity and phase of the VUV part of the supercontinuum from Fig. 4(b). (d) The time-domain intensity of the VUV part of the supercontinuum from Fig. 4(b). The blue curve is the pulse, and the orange curve is the pulse after phase compensation.

where the angle brackets denote an ensemble average over the independent simulations. If the electric fields had perfectly equal phase and intensity from shot to shot (i.e., are coherent), then the value of $|g_{pq}|$ would be 1, whereas a value of 0 indicates completely random phases between different laser shots. Figures 5(b) and 5(a) show the spectrum and the value $|g_{pq}|$ for propagation corresponding to Fig. 3(b)(i). The whole continuum is fully coherent. The VUV part, which has a simple phase structure as shown in Fig. 5(c), corresponds to a pulse of duration ~1 fs at the fiber output, even without any additional pulse compression, suggesting that this source could be used as a source of tunable few-femtosecond pulses in the VUV. If the phase is fully compensated, the duration reduced to 500 asec [Fig. 5(d)].

V. SUMMARY

We have demonstrated the generation of ultrashort VUV dispersive waves in He- and Ne-filled hollow-core kagome-style photonic crystal fiber. The emission is tunable from 120 to 200 nm, with efficiencies exceeding 1% and VUV pulse energies in excess of 50 nJ. We have also reported the generation of a three-octave-wide supercontinuum extending from the vacuum ultraviolet (VUV) to the near-infrared,

spanning at least 113–1000 nm (i.e., 11 − 1.2 eV). Numerical simulations have demonstrated that the supercontinuum arises from an interaction between dispersive-wave emission, soliton recoil, recompression, and plasma-induced soliton blueshift, causing the solitons to "bounce" from the fiber zero dispersion frequency and emit multiple VUV dispersive waves. Modeling also showed that the supercontinuum should be fully coherent. The VUV part possesses a simple phase structure having a duration of ∼500 asec if the phase is fully compensated.

[1] G. Sansone, F. Kelkensberg, J. F. Pérez-Torres, F. Morales, M. F. Kling, W. Siu, O. Ghafur, P. Johnsson, M. Swoboda, E. Benedetti, F. Ferrari, F. Lépine, J. L. Sanz-Vicario, S. Zherebtsov, I. Znakovskaya, A. L'Huillier, M. Y. Ivanov, M. Nisoli, F. Martín, and M. J. J. Vrakking, Electron localization following attosecond molecular photoionization, Nature **465**, 763 (2010).

[2] S. Lünnemann, A. I. Kuleff, and L. S. Cederbaum, Ultrafast charge migration in 2-phenylethyl-N,N-dimethylamine, Chem. Phys. Lett. **450**, 232 (2008).

[3] M. Drescher, M. Hentschel, R. Kienberger, M. Uiberacker, V. Yakovlev, A. Scrinzi, T. Westerwalbesloh, U. Kleineberg, U. Heinzmann, and F. Krausz, Time-resolved atomic inner-shell spectroscopy, Nature (London) **419**, 803 (2002).

[4] F. Remacle, M. Nest, and R. D. Levine, Laser Steered Ultrafast Quantum Dynamics of Electrons in LiH, Phys. Rev. Lett. **99**, 183902 (2007).

[5] M. F. Kling, C. Siedschlag, A. J. Verhoef, J. I. Khan, M. Schultze, T. Uphues, Y. Ni, M. Uiberacker, M. Drescher, F. Krausz, and M. J. J. Vrakking, Control of electron localization in molecular dissociation, Science **312**, 246 (2006).

[6] N. Tamai and H. Miyasaka, Ultrafast dynamics of photochromic systems, Chem. Rev. **100**, 1875 (2000).

[7] F. Reinert and S. Hüfner, Photoemission spectroscopy—From early days to recent applications, New J. Phys. **7**, 97 (2005).

[8] S. J. Hanna, P. Campuzano-Jost, E. A. Simpson, D. B. Robb, I. Burak, M. W. Blades, J. W. Hepburn, and A. K. Bertram, A new broadly tunable (7.4−10.2eV) laser based VUV light source and its first application to aerosol mass spectrometry, Int. J. Mass Spectrom. **279**, 134 (2009).

[9] M. Labat, M. Bellaveglia, M. Bougeard, B. Carré, F. Ciocci, E. Chiadroni, A. Cianchi, M. E. Couprie, L. Cultrera, M. Del Franco, G. Di Pirro, A. Drago, M. Ferrario, D. Filippetto, F. Frassetto, A. Gallo, D. Garzella, G. Gatti, L. Giannessi, G. Lambert *et al.*, High-Gain Harmonic-Generation Free-Electron Laser Seeded by Harmonics Generated in Gas, Phys. Rev. Lett. **107**, 224801 (2011).

[10] N. Y. Joly, P. Hölzer, J. Nold, W. Chang, J. C. Travers, M. Labat, M.-E. Couprie, and P. St. J. Russell (unpublished).

[11] M. Nest, F. Remacle, and R. D. Levine, Pump and probe ultrafast electron dynamics in LiH: a computational study, New J. Phys. **10**, 025019 (2008).

[12] V. Petrov, F. Noack, D. Shen, F. Pan, G. Shen, X. Wang, R. Komatsu, and V. Alex, Application of the nonlinear crystal SrB_4O_7 for ultrafast diagnostics converting to wavelengths as short as 125 nm, Opt. Lett. **29**, 373 (2004).

[13] H. Zhou, W. Li, L. Shi, D. Wang, L. Ding, and H. Zeng, Efficient generation of vacuum and extreme ultraviolet pulses, Laser Phys. Lett. **11**, 025402 (2014).

[14] M. Beutler, M. Ghotbi, F. Noack, and I. V. Hertel, Generation of sub-50-fs vacuum ultraviolet pulses by four-wave mixing in argon, Opt. Lett. **35**, 1491 (2010).

[15] F. Benabid, J. C. Knight, G. Antonopoulos, and P. St. J. Russell, Stimulated Raman scattering in hydrogen-filled hollow-core photonic crystal fiber, Science **298**, 399 (2002).

[16] J. C. Travers, W. Chang, J. Nold, N. Y. Joly, and P. St. J. Russell, Ultrafast nonlinear optics in gas-filled hollow-core photonic crystal fibers [Invited], J. Opt. Soc. Am. B **28**, A11 (2011).

[17] P. St. J. Russell, P. Hölzer, W. Chang, A. Abdolvand, and J. C. Travers, Hollow-core photonic crystal fibres for gas-based nonlinear optics, Nat. Photonics **8**, 278 (2014).

[18] N. Y. Joly, J. Nold, W. Chang, P. Hölzer, A. Nazarkin, G. K. L. Wong, F. Biancalana, and P. St. J. Russell, Bright Spatially Coherent Wavelength-Tunable Deep-Uv Laser Source Using an Ar-Filled Photonic Crystal Fiber, Phys. Rev. Lett. **106**, 203901 (2011).

[19] K. F. Mak, J. C. Travers, P. Hölzer, N. Y. Joly, and P. St. J. Russell, Tunable vacuum-UV to visible ultrafast pulse source based on gas-filled kagome-PCF, Opt. Express **21**, 10942 (2013).

[20] R. R. Alfano and S. L. Shapiro, Observation of Self-Phase Modulation and Small-Scale Filaments in Crystals and Glasses, Phys. Rev. Lett. **24**, 592 (1970).

[21] P. B. Corkum, C. Rolland, and T. Srinivasan-Rao, Supercontinuum Generation in Gases, Phys. Rev. Lett. **57**, 2268 (1986).

[22] R. L. Fork, W. J. Tomlinson, C. V. Shank, C. Hirlimann, and R. Yen, Femtosecond white-light continuum pulses, Opt. Lett. **8**, 1 (1983).

[23] A. Brodeur and S. L. Chin, Band-Gap Dependence of the Ultrafast White-Light Continuum, Phys. Rev. Lett. **80**, 4406 (1998).

[24] M. Kolesik, G. Katona, J. V. Moloney, and E. M. Wright, Physical Factors Limiting the Spectral Extent and Band Gap Dependence of Supercontinuum Generation, Phys. Rev. Lett. **91**, 043905 (2003).

[25] N. Boling, A. Glass, and A. Owyoung, Empirical relationships for predicting nonlinear refractive index changes in optical solids, IEEE J. Quantum Electron. **14**, 601 (1978).

[26] N. Aközbek, S. A. Trushin, A. Baltuška, W. Fuß, E. Goulielmakis, K. Kosma, F. Krausz, S. Panja, M. Uiberacker, W. E. Schmid, A. Becker, M. Scalora, and M. Bloemer, Extending the supercontinuum spectrum down to 200 nm with few-cycle pulses, New J. Phys. **8**, 177 (2006).

[27] F. Reiter, U. Graf, E. E. Serebryannikov, W. Schweinberger, M. Fiess, M. Schultze, A. M. Azzeer, R. Kienberger, F. Krausz, A. M. Zheltikov, and E. Goulielmakis, Route to Attosecond Nonlinear Spectroscopy, Phys. Rev. Lett. **105**, 243902 (2010).

[28] H. Nishioka, W. Odajima, K. Ueda, and H. Takuma, Ultrabroadband flat continuum generation in multichannel propagation of terrawatt Ti:sapphire laser pulses, Opt. Lett. **20**, 2505 (1995).

[29] P. St. J. Russell, Photonic-crystal fibers, J. Light. Technol. **24**, 4729 (2006).

[30] J. M. Dudley, G. Genty, and S. Coen, Supercontinuum generation in photonic crystal fiber, Rev. Mod. Phys. **78**, 1135 (2006).

[31] J. M. Dudley and J. R. Taylor, *Supercontinuum Generation in Optical Fibers* (Cambridge University Press, Cambridge, UK, 2010).

[32] A. A. Amorim, M. V. Tognetti, P. Oliveira, J. L. Silva, L. M. Bernardo, F. X. Kärtner, and H. M. Crespo, Sub-two-cycle pulses by soliton self-compression in highly nonlinear photonic crystal fibers, Opt. Lett. **34**, 3851 (2009).

[33] A. A. Voronin and A. M. Zheltikov, Soliton-number analysis of soliton-effect pulse compression to single-cycle pulse widths, Phys. Rev. A **78**, 063834 (2008).

[34] P. Beaud, W. Hodel, B. Zysset, and H. P. Weber, Ultrashort pulse propagation, pulse breakup, and fundamental soliton formation in a single-mode optical fiber, IEEE J. Quantum Electron. **23**, 1938 (1987).

[35] Y. Kodama and A. Hasegawa, Nonlinear pulse propagation in a monomode dielectric guide, IEEE J. Quantum Electron. **23**, 510 (1987).

[36] A. V. Husakou and J. Herrmann, Supercontinuum Generation of Higher-Order Solitons by Fission in Photonic Crystal Fibers, Phys. Rev. Lett. **87**, 203901 (2001).

[37] P. K. A. Wai, C. R. Menyuk, Y. C. Lee, and H. H. Chen, Nonlinear pulse propagation in the neighborhood of the zero-dispersion wavelength of monomode optical fibers, Opt. Lett. **11**, 464 (1986).

[38] S.-J. Im, A. Husakou, and J. Herrmann, High-power soliton-induced supercontinuum generation and tunable sub-10-fs VUV pulses from kagome-lattice HC-PCFs, Opt. Express **18**, 5367 (2010).

[39] S. P. Stark, J. C. Travers, and P. St. J. Russell, Extreme supercontinuum generation to the deep UV, Opt. Lett. **37**, 770 (2012).

[40] X. Jiang, N. Y. Joly, M. A. Finger, F. Babic, G. K. L. Wong, J. C. Travers, and P. St. J. Russell, Deep-ultraviolet to mid-infrared supercontinuum generated in solid-core ZBLAN photonic crystal fibre, Nat. Photonics **9**, 133 (2015).

[41] F. Belli, A. Abdolvand, W. Chang, J. C. Travers, and P. St. J. Russell, Vacuum-ultraviolet to infrared supercontinuum in hydrogen-filled photonic crystal fiber, Optica **2**, 292 (2015).

[42] P. Hölzer, W. Chang, J. C. Travers, A. Nazarkin, J. Nold, N. Y. Joly, M. F. Saleh, F. Biancalana, and P. St. J. Russell, Femtosecond Nonlinear Fiber Optics in the Ionization Regime, Phys. Rev. Lett. **107**, 203901 (2011).

[43] M. F. Saleh, W. Chang, P. Hölzer, A. Nazarkin, J. C. Travers, N. Y. Joly, P. St. J. Russell, and F. Biancalana, Theory of Photoionization-Induced Blueshift of Ultrashort Solitons in Gas-Filled Hollow-Core Photonic Crystal Fibers, Phys. Rev. Lett. **107**, 203902 (2011).

[44] W. Chang, A. Nazarkin, J. C. Travers, J. Nold, P. Hölzer, N. Y. Joly, and P. St. J. Russell, Influence of ionization on ultrafast gas-based nonlinear fiber optics, Opt. Express **19**, 21018 (2011).

[45] W. Chang, P. Hölzer, J. C. Travers, and P. St. J. Russell, Combined soliton pulse compression and plasma-related frequency upconversion in gas-filled photonic crystal fiber, Opt. Lett. **38**, 2984 (2013).

[46] V. I. Karpman, Radiation by solitons due to higher-order dispersion, Phys. Rev. E **47**, 2073 (1993).

[47] N. Akhmediev and M. Karlsson, Cherenkov radiation emitted by solitons in optical fibers, Phys. Rev. A **51**, 2602 (1995).

[48] J. N. Elgin, T. Brabec, and S. M. J. Kelly, A perturbative theory of soliton propagation in the presence of third order dispersion, Opt. Commun. **114**, 321 (1995).

[49] M. Erkintalo, Y. Q. Xu, S. G. Murdoch, J. M. Dudley, and G. Genty, Cascaded Phase Matching and Nonlinear Symmetry Breaking in Fiber Frequency Combs, Phys. Rev. Lett. **109**, 223904 (2012).

[50] F. Tani, J. C. Travers, and P. St. J. Russell, Multimode ultrafast nonlinear optics in optical waveguides: Numerical modeling and experiments in kagomé photonic-crystal fiber, J. Opt. Soc. Am. B **31**, 311 (2014).

[51] H. J. Lehmeier, W. Leupacher, and A. Penzkofer, Nonresonant third order hyperpolarizability of rare gases and N_2 determined by third harmonic generation, Opt. Commun. **56**, 67 (1985).

[52] E. A. J. Marcatili and R. A. Schmeltzer, Hollow metallic and dielectric waveguides for long distance optical transmission and lasers, Bell Syst. Tech. J. **43**, 1783 (1964).

[53] A. Börzsönyi, Z. Heiner, M. P. Kalashnikov, A. P. Kovács, and K. Osvay, Dispersion measurement of inert gases and gas mixtures at 800 nm, Appl. Opt. **47**, 4856 (2008).

[54] M. C. E. Huber and G. Tondello, Refractive index of He in the region 920–1910 Å, J. Opt. Soc. Am. **64**, 390 (1974).

[55] A. M. Perelomov, V. S. Popov, and M. V. Terent'ev, Ionization of atoms in an alternating electric field, Sov. Phys. JETP **23**, 924 (1966).

[56] F. A. Ilkov, J. E. Decker, and S. L. Chin, Ionization of atoms in the tunnelling regime with experimental evidence using Hg atoms, J. Phys. B At. Mol. Opt. Phys. **25**, 4005 (1992).

[57] M. Geissler, G. Tempea, A. Scrinzi, M. Schnürer, F. Krausz, and T. Brabec, Light Propagation in Field-Ionizing Media: Extreme Nonlinear Optics, Phys. Rev. Lett. **83**, 2930 (1999).

[58] L. F. Mollenauer, W. J. Tomlinson, R. H. Stolen, and J. P. Gordon, Extreme picosecond pulse narrowing by means of soliton effect in single-mode optical fibers, Opt. Lett. **8**, 289 (1983).

[59] F. DeMartini, C. H. Townes, T. K. Gustafson, and P. L. Kelley, Self-steepening of light pulses, Phys. Rev. **164**, 312 (1967).

[60] J. C. Travers, P. Hölzer, W. Chang, J. Nold, A. Nazarkin, N. Joly, and P. St. J. Russell, Phase-matching and gain of deep-UV dispersive-wave generation, in *CLEO/Europe and EQEC 2011 Conference Digest, OSA Technical Digest (CD)* (Optical Society of America, Washington, DC, 2011), p. CJ3_1.

[61] M. F. Saleh and F. Biancalana, Understanding the dynamics of photoionization-induced solitons in gas-filled hollow-core photonic crystal fibers, Phys. Rev. A. **84**, 063838 (2011).

[62] F. Biancalana, D. V. Skryabin, and A. V. Yulin, Theory of the soliton self-frequency shift compensation by the resonant radiation in photonic crystal fibers, Phys. Rev. E **70**, 016615 (2004).

[63] J. M. Dudley and S. Coen, Coherence properties of supercontinuum spectra generated in photonic crystal and tapered optical fibers, Opt. Lett. **27**, 1180 (2002).